Atom Indonesia

Journal homepage: http://atomindonesia.brin.go.id

Analysis of Alpha and Lithium-7 Particle Energy Deposition in BNCT using Geant4 Simulation

K. Charef[1*], F. Z. Ahlaf[2], Y. Khoulaki[1], D. Benchekroun[1], H. Harrass[1,3], I. Fathi[1,3], Y. Makhkhas[1]

[1]*Laboratory of High Energy Physics and Condensed Matter (PHEMAC), Faculty of Science Ain Chock. University Hassan II – Casablanca, Morocco*
[2]*Immuno-Genetics and Human Pathology laboratory, Faculty of Medicine and Pharmacy, Hassan II University of Casablanca, Morocco*
[3]*Biophysics service, Faculty of Medicine and Pharmacy, Hassan II University of Casablanca, Morocco*

ARTICLE INFO

Article history:
Received 27 July 2024
Received 22 October 2024
Accepted 24 October 2024

Keywords:

Boron Neutron Capture Therapy (BNCT)
Lithium-7 particles
Alpha particles
Geant4
Monte Carlo
Microdosimetric

ABSTRACT

This study investigates the microdosimetric characteristic of Boron Neutron Capture Therapy (BNCT) using high-fidelity Monte Carlo simulations to quantify the energy deposition distributions of alpha and lithium-7 particles within cellular structures. The Geant4 toolkit is utilized to model various physics lists and water representations, aiming to optimize the accuracy of BNCT simulations. Dosimetric and microdosimetric studies using these Monte Carlo techniques are conducted to examine the behavior of the produced alpha and lithium-7 particles and their energy deposition in different cellular compartments. Our findings contribute to the understanding of BNCT's effects at the cellular level, which is crucial for advancing treatment planning and minimizing side effects.

INTRODUCTION

Boron Neutron Capture Therapy (BNCT) is an emerging binary cancer treatment modality that shows significant promise for treatment of aggressive and invasive tumors such as glioblastoma multiforme, melanoma, and head and neck cancers [1,2]. This technique relies on the synergistic action of two relatively non-toxic components: a tumor-selective boron-10 (^{10}B) carrier agent and a beam of low-energy thermal neutrons. Upon thermal neutron capture, ^{10}B nuclei capture these neutrons, they undergo the ^{10}B (n, α)^{7}Li nuclear reaction, producing high Linear Energy Transfer (LET) particles, namely an alpha particle (^{4}He) with an energy of 1.47 MeV or 1.78 MeV (in 6.3 % of cases) and a lithium-7 (^{7}Li) nucleus with an energy of 0.84 MeV or 1.01 MeV respectively [3,4] (Fig. 1). The ^{10} B(n,α)^{7} Li reaction is described by Eq. (1) and Eq. (2).

$$^{1}n + {}^{10}B \rightarrow {}^{10}B^{*} \rightarrow {}^{7}Li(0.84\,MeV) + \alpha\,(1.47MeV) + \gamma\,(0.48MeV)\,(93.7\%) \quad (1)$$

$$^{1}n + {}^{10}B \rightarrow {}^{10}B^{*} \rightarrow {}^{7}Li(1.01MeV) + \alpha\,(1.78MeV)(6.3\%) \quad (2)$$

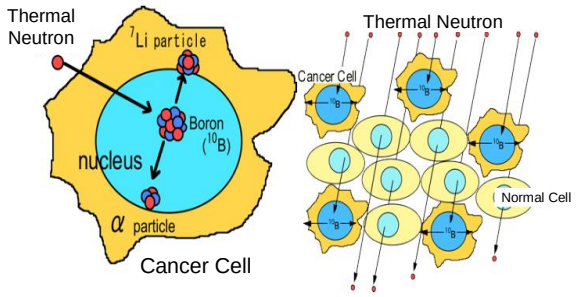

Fig. 1. Concept of BNCT [4].

The principal advantage of BNCT lies in the short path lengths of the high-LET charged particles in biological tissues, which are typically limited to a few cell diameters (approximately 5-9 µm) [4]. This allows the particle's cytotoxic effects to be confined within a small volumetric region around the ^{10}B delivery sites. By selectively delivering sufficient concentration of ^{10}B tumor cells using biochemically targeted agents, followed by irradiation with epithermal neutron beams, it is theoretically possible to destroy these loaded cells through direct energy deposition, while sparing adjacent healthy tissues from collateral damage [5].

Currently, two main ^{10}B-containingcompounds are utilized in BNCT: sodium borocaptate (BSH) and boronophenylalanine (BPA). BSH tends to

*Corresponding author.
E-mail address: khadija.charef2-etu@etu.univh2c.ma
DOI: https://doi.org/10.55981/aij.2025.1501

accumulate around tumor cell membranes, due to weaknesses in the neoplastic cell vascular architecture. In contrast, BPA, which is structurally analogous to phenylalanine, is capable of crossing the blood-brain barrier, allowing it to target melanoma cells as well as infiltrate intracranial lesions like glioblastomas where it accumulates in proximity to nuclear regions [6].

Although BNCT presents a theoretically promising therapeutic strategy, several challenges hinder its clinical implementation. These include achieving therapeutically effective tumor-to-normal tissue ^{10}B concentrations ratios, ensuring adequate neutron penetration into tumors using epithermal neutron sources, and accounting for the heterogeneous microdistribution of ^{10}B at the cellular level. These factors directly influence the radiation dosimetry and, consequently, the biological effectiveness of the high-LET particles generated during treatment [7].

Monte Carlo-based computational microdosimetry using radiation transport codes like Geant4 provides a powerful approach to model the stochastic energy deposition processes arising from BNCT reactions at sub-cellular scales. By accurately simulating the emission and slowing down of alpha and lithium particles generated from ^{10}B (n, α) ^{7}Li events within detailed multi-cellular cluster geometries, it becomes possible to compute microdosimetric quantities such as lineal energy distributions which are strongly correlated with DNA damage induction and cellular survival rates [8].

The present work aims to leverage high-fidelity Geant4 simulations to quantify the spatial energy deposition profiles of alpha and lithium particles resulting from BNCT reactions within monocellular tissue models. We investigate the influence of different physics models, including the standard electromagnetic physics list and the Geant4-DNA extension, which is specifically designed for low-energy interactions. Furthermore, we examine the impact of water modeling approaches, comparing the pre-defined G4_WATER material with explicit chemical definitions using H_2O molecular formula, on the resulting energy deposition patterns [9].

Through rigorous validation against established experimental data, detailed Monte Carlo simulations can elucidate critical microdosimetric characteristics that ultimately dictate the biological effects in both cancerous and healthy cell populations during BNCT irradiations. This can support the development of optimized clinical protocols, enhancing tumor control probability while minimizing collateral damage to normal tissues. In doing so, this binary therapeutic approach may advance toward broader clinical adoption as an effective treatment for difficult-to-treat tumor types [10].

The main objective of this study is to use high-fidelity Monte Carlo simulations to quantify the energy deposition distributions of alpha particles and lithium-7 resulting from BNCT reactions in realistic single-cell geometies. This study evaluates carious scenarios of boron accumulation to elucidate the influence of subcellular boron localization on microdosimetric outcomes. Furthermore, the study aims to identify optimal combinations of Geant4 physics lists and material definitions to accurately simulate the interaction and deceleration of high Linear Energy Transfer (LET) charged particles in biological media. Validation against existing benchmark data will ensure the reliability of the dosimetric predictions. The results obtained are expected to deepen the understanding of the biophysical mechanisms underlying BNCT-induced effects and inform the design of more effective treatment plans that maximize tumor control while preserving surrounding healthy tissues [11,12].

METHODOLOGY

Geant4 toolkit

GEANT4 is a Monte Carlo software toolkit designed for the simulation of particles. Its core is composed of routines programmed in C++. GEANT4 can simulate the interaction of various particles types as they interact with different materials. The acronym GEANT4 stands for Geometry and Tracking, with the version discussed here being the fourth major release. Although GEANT4 has a wide range of applications, it is commonly utilized in high-energy physics, medical physics, and space sciences, rather than in nuclear reactor physics [13]. To perform a GEANT4 simulations, users are required to define at least three primary components: (1) the physics processes relevant to the simulation, including those associated with each particle; (2) the geometry of the system; and (3) the properties of the primary particle to be simulated. Among these, the definition of the physical models and the construction of geometry are two main aspects of GEANT4. A thorough understanding of both is essential for the effective use of the toolkit [14,15].

Target model

A simplified single-cell model (Fig. 2) was utilized to calculate the behavior of alpha particles and Lithium-7 nuclei generated through boron

neutron capture reactions. The model consisted of distinct compartments representing the nucleus, cytoplasm A, cytoplasm B, and the cell membrane. The dimensions of each compartment were defined based on typical cellular anatomy, as shown in Table 1.

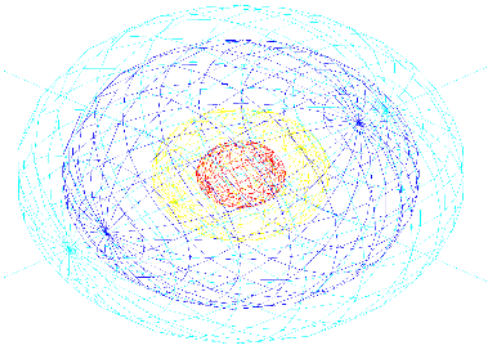

Fig. 2. Mono cell model.

Table 1. Cell compartment thickness.

Area	nucl	cyt (A)	cyt (B)	cellm
Thickness	1.0 µm	1.0 µm	2.0 µm	1.0 µm

note:
nucl : nucleus (red).
cyt(A) : cytoplasm A (yellow).
cyt(B) : cytoplasm B (blue).
cellm : cell membrane (cyan).

To examine the spatial distributions of the alpha particles and Lithium-7 nuclei, simulations were conducted assuming boron-10 accumulation in distinct subcellular locations: the cell membrane for sodium borocaptate (BSH) and cytoplasm A for p-boronophenylalanine (BPA), with a uniform ^{10}B concentration of 24 ppm within the cell. Neutrons with an energy of approximately 0.025 eV, which is typical for BNCT applications, were used. Using this model, key parameters were evaluated for each boron compound, including the number of alpha and Lithium-7 particles generated, their respective ranges, Linear Energy Transfer (LET), and the resulting spatial dose distribution. This single-cell model provides a simplified yet informative framework for elucidating the microdosimetric characteristics of BNCT reactions, enabling quantification of particle behavior and energy depositions within individual subcellular compartments. The model can be extended to multicellular systems and adapted for different ^{10}B distribution patterns, offering valuable insight for optimizing BNCT treatment planning.

Geant4 physics lists for simulating BNCT reactions

The application of Geant4 to BNCT simulations gained significant momentum in recent years due to its versatility and accuracy [16]. A critical component of Monte Carlo simulations in Geant4 is the selection of an appropriate physics list to accurately model particle interactions within biological matter. In this study, we evaluated several physics lists relevant to the simulation of alpha particles, lithium-7 nuclei, and thermal neutrons produced through boron neutron capture reactions.

In our work, we systematically evaluated and compared multiple physics lists to identify the configuration that best represents the microdosimetric phenomena associated with BNCT reactions in biological media. Particular attention was given to accurately reproducing the ranges of charged particles and their corresponding energy deposition profile at both cellular and subcellular scales. The objective was to optimize the Monte Carlo modeling framework to enhance the predictive accuracy of BNCT-induced biological effects. Specifically, three key physics lists were employed and analyzed in detail [17,18]:

Geant4-DNA, this extension of the Geant4 toolkit is specifically designed to simulate particle interactions with biological matter at the molecular and cellular scale. It incorporates detailed models of physical, chemical, and biological processes, enabling the simulation of both direct and indirect DNA damage caused by ionizing radiation. Geant4-DNA is particularly useful for applications in radiobiology, radiotherapy, and radiation protection.

G4QGSP_BIC, this physics list in Geant4 integrates multiple models to simulate hadronic interactions across a broad energy spectrum. The QGSP (Quark-Gluon String Precompound) model handles high-energy interactions, while the BIC (Binary Cascade) model is applied to medium-energy interactions, particularly effective for nucleon-induced reactions. G4QGSP-BIC is well-suited for simulating complex interactions involving hadrons and ions, making it a versatile choice for applications in both particle physics and medical physics, including hadron therapy and BNCT.

G4QGSP_BIC_HP, this physics list extends G4QGSP_BIC by incorporating High-Precision (HP) models specifically designed for low-energy neutron interactions. The HP component utilized evaluated nuclear data libraries to provide more accurate cross-section information and interaction probabilities. This enhancement is particularly important for applications such as BNCT (Boron Neutron Capture Therapy) where the accurate modeling of thermal and epithermal neutron interaction is essential for predicting dose distributions and treatment efficacy.

Water in Geant4 simulations: G4_WATER vs. H_2O

In Geant4, water can be declared in two distinct ways: G4_WATER and H_2O. Although both represent the same water molecule, they differ in implementation and are used depending on the specific requirements of the simulation. G4_WATER is a predefined material available within the Geant4NIST (National Institute of Standards and Technology) material database. This implementation uses precise compositions and physical properties of water, based on experimental data. G4_WATER is recommended for general-purpose simulations, especially when high fidelity and realism in material behavior are essential. In contrast, H_2O refers to a user-defined material, in which chemical composition and chemical properties of water are manually specified. This approach can be useful in specific cases, such as when studying the impact of slight variations in the composition or density of water on the simulation results. In the present study, both G4_WATER and H_2O were utilized to define water in the geometric models. This dual approach enabled a comparative analysis of the energy deposition results associated with each declaration, thereby evaluating the potential influence of material definition on the simulation outcomes [19].

RESULTS

The deposited energies observed in the simulated cell with both alpha particles and lithium ions were identical when using the Geant4-DNA and G4QGSP_BIC physics lists, whereas a slight deviation is observed with the G4QGSP_BIC_HP list. This consistent pattern across both particle types can be attributed to several factors.

Dominant interaction mechanisms: Both alpha particles and lithium ions primarily interact with matter through electromagnetic processes, particularly ionization and excitation. In the energy range considered, these are the dominant modes of energy loss, and both Geant4-DNA and G4QGSP_BIC physics lists accurately model this interaction, resulting in consistent energy deposition outcomes.

Energy range specificity: Within the specific energy range relevant to this simulation, the electromagnetic interaction models implemented in Geant4-DNA and G4QGSP_BIC are likely very similar or identical for alpha particles and lithium ions. This overlap leads to nearly indistinguishable predictions of energy deposition between the two physics lists.

Precision of electromagnetic models: The electromagnetic physics models in Geant4 have undergone extensive validation and optimization over the years. As a result, they provide high accuracy across different physics lists for well-characterized particles such as alpha particles and lithium ions. Limited impact of hadronic processes: Although G4QGSP_BIC includes hadronic interaction model, these processes are negligible for alpha particles and lithium ions within the studied energy range and simulation geometry. This explains the results obtained using Geant4-DNA, the latter of which emphasizes electromagnetic and low-energy processes [20].

However, the slight difference observed with G4QGSP_BIC_HP for both particle types can be attributed to its unique features.

Neutron treatment: G4QGSP_BIC_HP uses more accurate data for high-precision (HP) neutrons. Although neither alpha particles nor Lithium ions interact directly through the strong interaction, they can produce secondary neutrons under certain conditions, which could slightly influence the overall results. Nuclear reactions: At certain energies, nuclear reactions involving alpha particles or lithium ions may occur. The G4QGSP_BIC_HP list may model these reactions with greater detail or different assumptions compared to other physics leading to slight variations in simulation outcomes. Increased precision at low energy: The HP component enhances the modeling of low-energy interactions. This potentially affects how secondary particles and end-of-range processes-particularly those occurring in the subcellular structure are treated, resulting in marginal differences in energy deposition. Threshold effects and material interactions: Variations in production thresholds for secondary particles, as well as differences in how interactions with specific materials are handled near geometric boundaries, may contribute to discrepancies in deposited energy. Statistical fluctuations: If the observed differences are minor, it is also important to consider the inherent statistical fluctuations associated with Monte Carlo simulations, which could affect results for both particle types.

The consistency between Geant4-DNA and G4QGSP_BIC for both alpha particles and lithium ions suggests that either physics list is suitable for simulating interactions of these particles under similar conditions. However, the slight differences observed with G4QGSP_BIC_HP underscore the importance of choosing the appropriate physics list based on the specific application and the required

level of precision, regardless of the particle type. These findings highlight the necessity of careful evaluation and, where possible, experimental validation when relying on simulations for critical applications. Additionally, simulation parameters such as geometry, material composition, and energy range should be carefully considered, as they can significantly influence the convergence of results across different physics lists for both alpha particles and lithium ions [21].

Energy distribution between G4QGSP_BIC_HP and Geant4-DNA using H_2O

In this section, we present a comparative analysis of the energy distribution patterns obtained using two different physics lists: G4QGSP_BIC_HP and Geant4-DNA, both applied to a water model represented as H_2O. This comparison aims to highlight the similarities and differences in energy deposition predictions between these two approaches, providing insights into their relative strengths and potential limitations for simulating alpha particle and lithium ions interactions in cellular structures.

The following plots (Figs. 3-10) illustrate the energy distribution within various subcellular compartments: the nucleus, cytoplasm A, cytoplasm B, and the cell membrane. Each plot represents a specific cellular region, allowing for a detailed assessment of how the selected physics list influences the predicted energy deposition across different cellular domains.

Study system with alpha particles

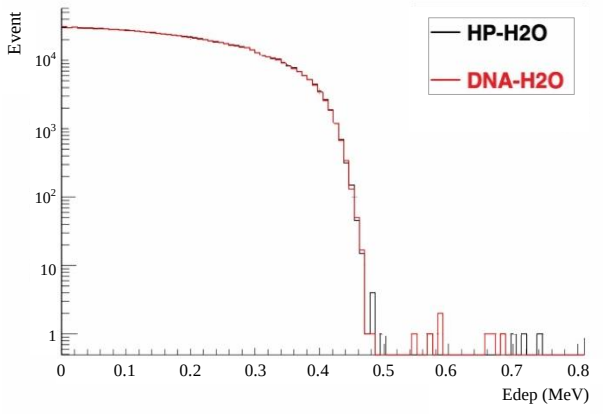

Fig. 3. Distribution of deposit energy in Nucleus.

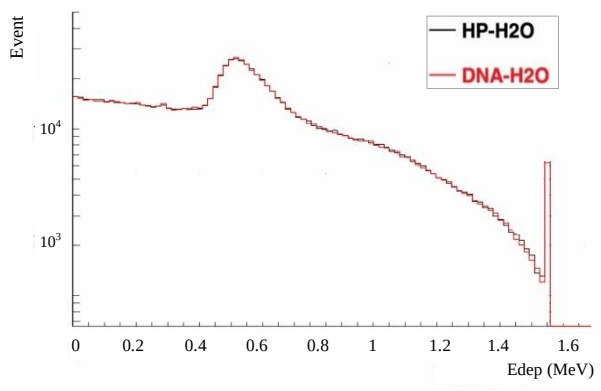

Fig. 4. Distribution of deposit energy in Cyto. A.

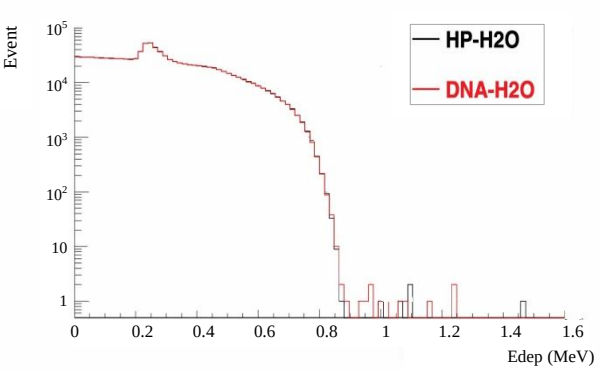

Fig. 5. Distribution of deposit energy in Cyto. B.

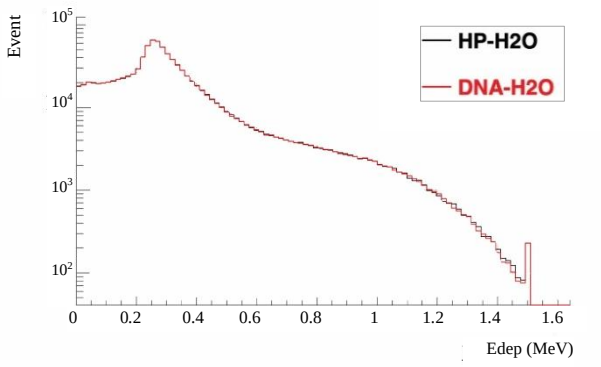

Fig. 6. Distribution of deposit energy in CellM.

Study system with lithium ion

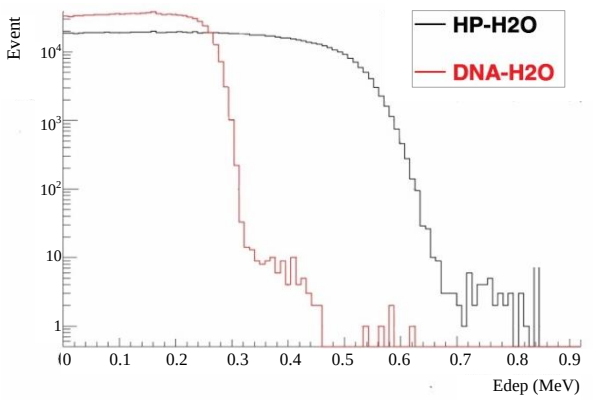

Fig. 7. Distribution of deposited energy in Nucleus.

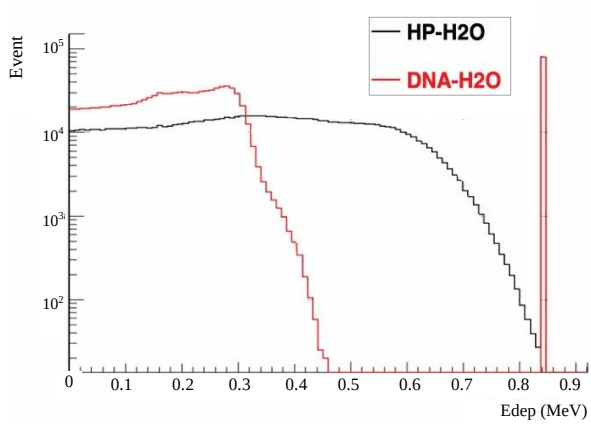

Fig. 8. Distribution of deposited energy in Cyto. A.

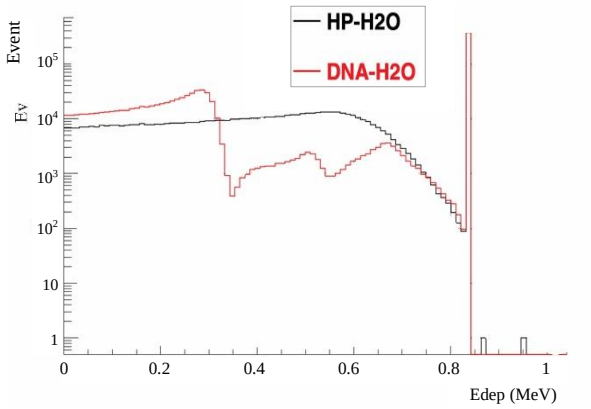

Fig. 9. Distribution of deposited energy in Cyto. B.

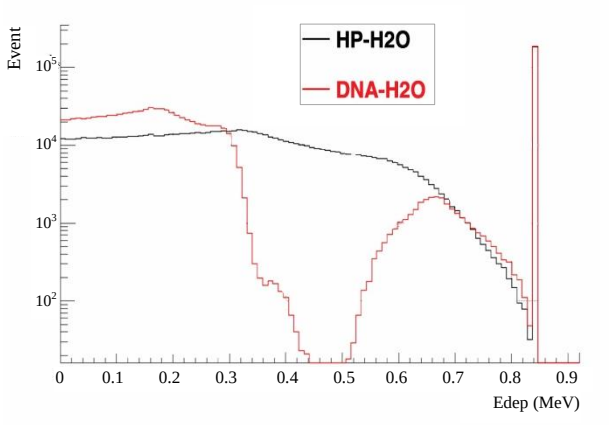

Fig. 10. Distribution of deposited energy in CellM.

Energy distribution between G4QGSP_BIC_HP and Geant4-DNA using G4_Water

Following our analysis using the H_2O model, we now focus on comparing energy distributions using the G4_Water material definition in Geant4. This section presents an analysis parallel to that of Section 1.1, with the key difference of utilizing the pre-defined G4_Water material instead of the explicitly defined H_2O.

The purpose of this comparison is twofold: (1) to examine how the choice of water model (H_2O vs G4_Water) affects the energy deposition patterns, and (2) to further explore the differences between the G4QGSP_BIC_HP and Geant4-DNA physics lists when applied to an alternative water representation. As in the previous section, we present plots showing the energy distribution within the nucleus, cytoplasm A, cytoplasm B, and the cell membrane. These plots (Figs. 11-18) allow for a direct comparison not only between the two physics lists but also between the simulation results obtained using H_2O and G4_Water models.

Study system with Alpha particles

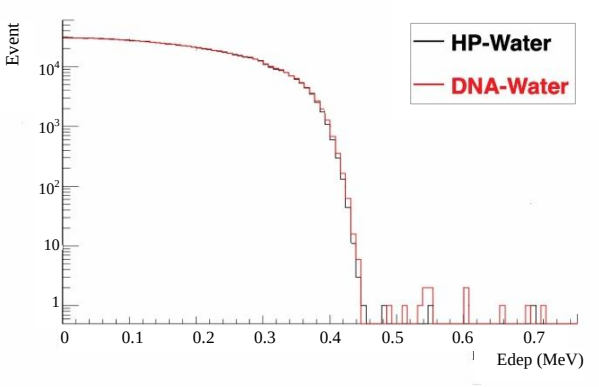

Fig. 11. Distribution of deposited energy in Nucleus.

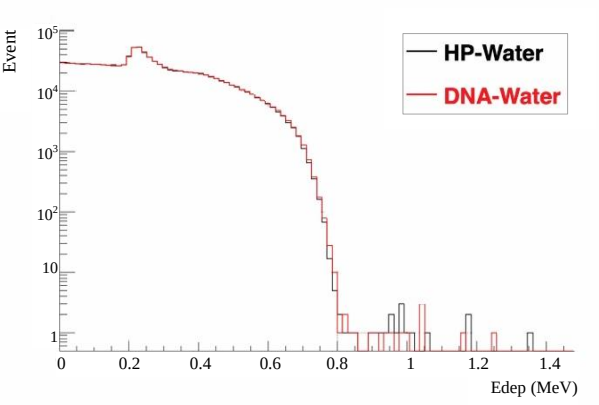

Fig. 12. Distribution of deposited energy in Cyto. A.

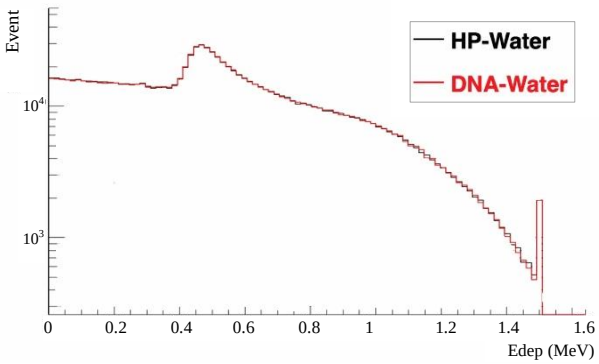

Fig. 13. Distribution of deposited energy in Cyto. B.

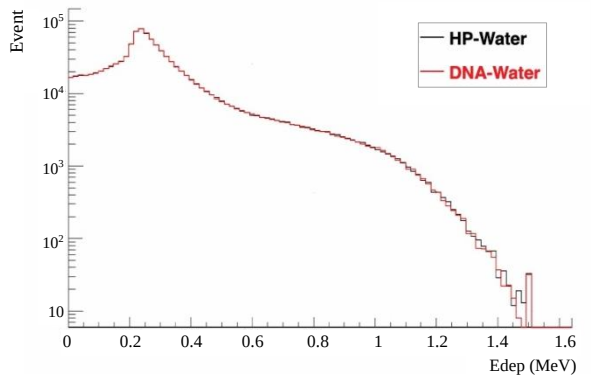

Fig. 14. Distribution of deposited energy in CellM.

Study system with lithium-ion

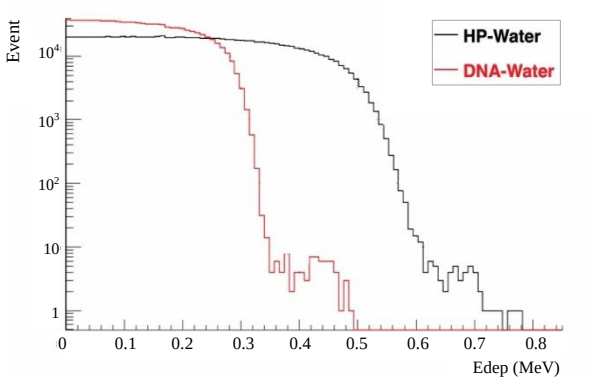

Fig. 15. Distribution of deposited energy in Nucleus.

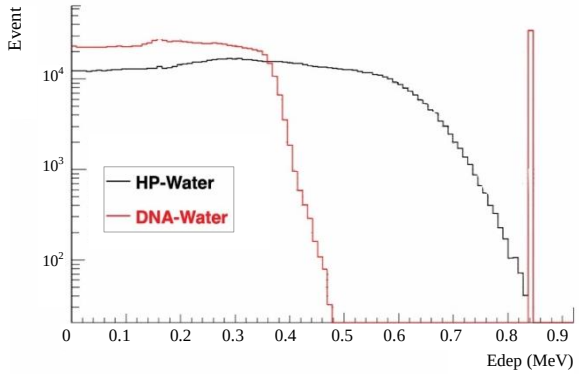

Fig. 16. Distribution of deposited energy in Cyto. A.

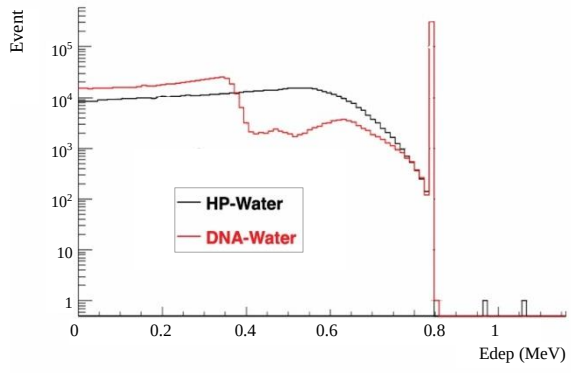

Fig. 17. Distribution of deposited energy in Cyto. B.

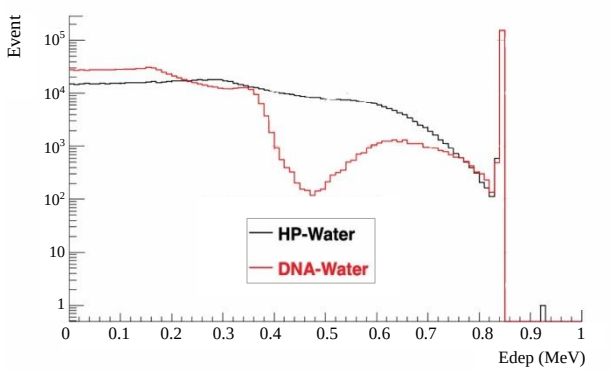

Fig. 18. Distribution of deposited energy in CellM.

Overall similarity, the graphs show a strong similarity between the G4QGSP_BIC_HP and Geant4-DNA models for both H_2O and G4_Water materials. This similarity is observed in the distribution of deposited energy across various cellular structures.

Comparison of cellular structures, the study focuses on the energy distribution within the nucleus, cytoplasm A, cytoplasm B, and cell membrane. Each graph corresponds to a specific compartment, with the radiation source positioned within that same compartment to maintain consistency across the simulation.

Specific differences, minor variations can be observed between the models, particularly for rare events or at high energy levels. These differences might be more pronounced in certain cellular structures compared to others.

Material influence, the comparison between H_2O and G4_Water generally yields similar results. However, slight differences in curve shapes and peak positions suggest that the choice of water model can have a subtle influence on simulation outcomes.

Implications, the observed consistency between G4QGSP_BIC_HP and Geant4-DNA validates the reliability of both physics lists for simulating alpha particle and lithium-ion interactions in water. While the choice between H_2O and G4_Water seems to have minimal impact but could be important for very precise studies.

Energy deposition patterns using Geant4-DNA physics list

The distribution of deposited energy in different cell compartments for various source positions is presented in Figs. 19-28. Each graph corresponds to a specific target compartment, with the radiation source placed within the same compartment to ensure the consistency of the analysis.

Study system with alpha particles

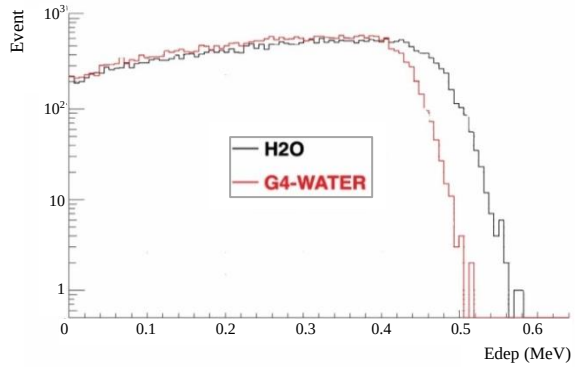

Fig. 19. Distribution of deposited energy in Nucleus: Nucleus Source.

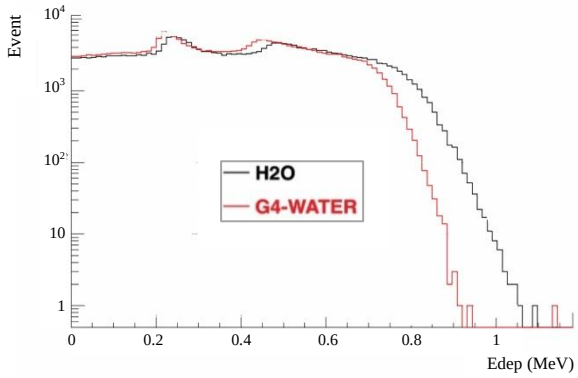

Fig. 20. Distribution of deposited energy in Cyto. A: Cyto. A Source.

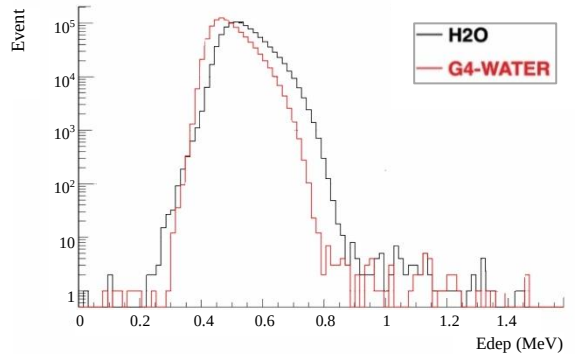

Fig. 21. Distribution of deposited energy in Cyto. B: Cyto. B Source.

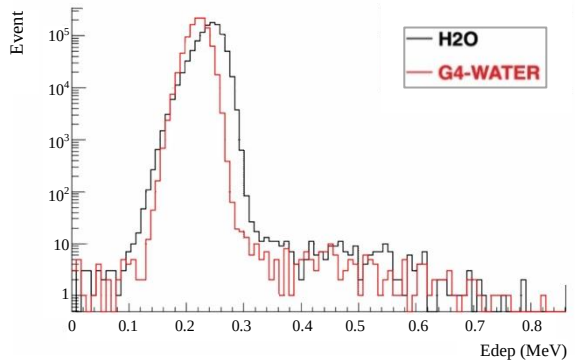

Fig. 22. Distribution of deposited energy in CellM: CellM Source.

Table 2a. Percentage of Deposited Energy using H_2O.

H_2O	Cell Central				
Source	Nucl	Cyt(A)	Cyt(B)	CellM	Tot.
Nucl	10.44	16.94	33.39	15.95	76.74
Cyt(A)	3.42	18.35	36.22	16.00	74.01
Cyt(B)	0.95	6.30	33.78	18.16	62.80
CellM	0.60	4.10	27.39	21.42	53.54

Table 2b. Percentage of Deposited Energy using G4_Water.

G4_Water	Cell Central				
Source	Nucl	Cyt(A)	Cyt(B)	CellM	Tot.
Nucl	9.79	15.71	30.28	14.71	70.50
Cyt(A)	3.20	17.07	33.09	14.91	68.28
Cyt(B)	0.87	5.80	34.82	17.21	58.71
CellM	0.56	3.79	25.65	20.26	50.28

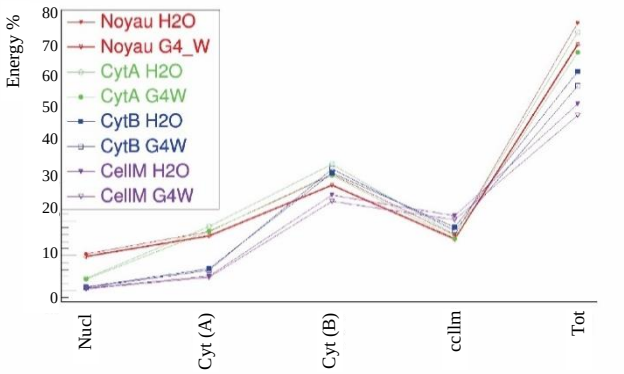

Fig. 23. Comparison of deposited energy percentages: H_2O vs G4_Water.

Table 2 presents the percentage of energy deposited in each cellular compartment for different source positions, comparing the results obtained using the H_2O and G4_WATER material models. The table is divided into two parts: Table 2a presents data for the H_2O model, while Table 2b corresponds to the G4_WATER model. Significant differences are observed depending on the source location and target compartment, as illustrated in Fig 23, which provides a comparative overview of these variations.

These results demonstrate the impact of cellular geometry and selected water models on energy deposition patterns, highlighting the importance of accurate modeling in micro-dosimetry simulations.

Study system with lithium-ion

The percentage of energy deposited in each compartment for various source positions is displayed in Tables. 3 (a) and (b). Remarkable variations are noticed based on the source placement and the compartment targeted as shown in Fig. 28.

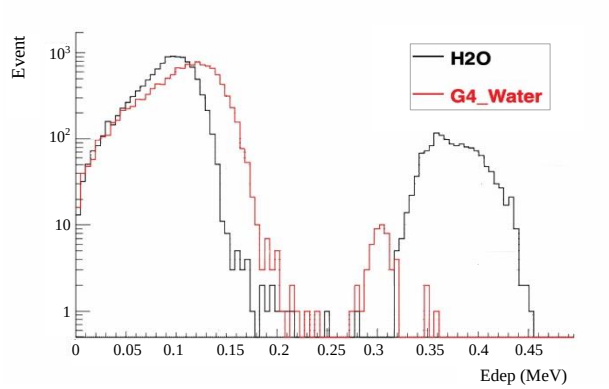

Fig. 24. Distribution of deposited energy in nucleus: Nucleus source.

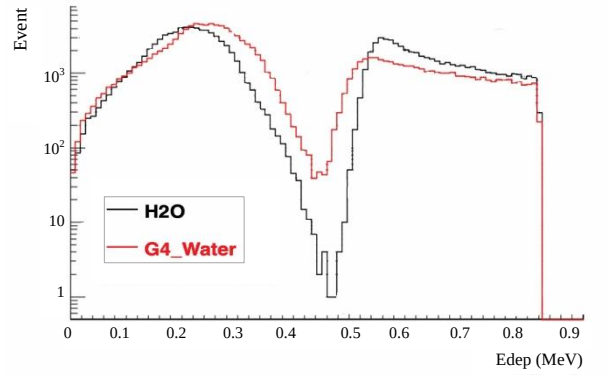

Fig. 25. Distribution of deposited energy in Cyto. A: Cyto. A source.

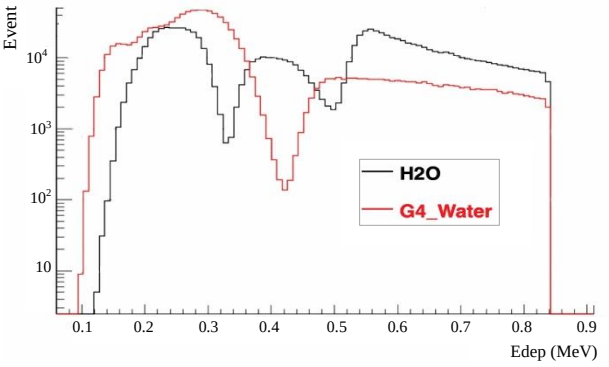

Fig. 26. Distribution of deposited energy in Cyto. B: Cyto. B source.

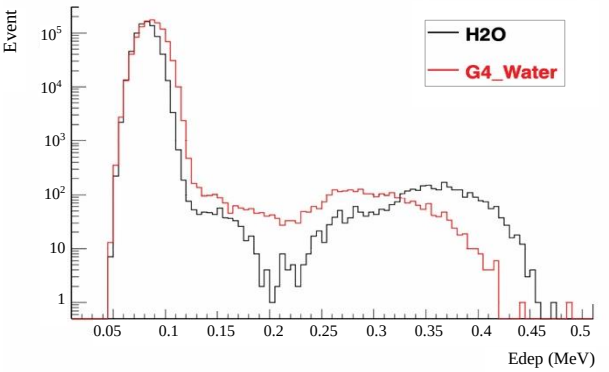

Fig. 27. Distribution of deposited energy in CellM: CellM source.

Table 3a. Percentage of Deposited Energy using H_2O.

H_2O	Cell central				
Source	Nucl	Cyt(A)	Cyt(B)	CellM	Tot.
Nucl	15.80	19.92	30.06	7.48	73.28
Cyt(A)	2.72	27.56	52.28	3.81	86.38
Cyt(B)	0.41	5.81	54.50	11.02	71.75
CellM	0.18	1.13	19.89	35.06	56.27

Table 3b. Percentage of Deposited Energy using G4_Water.

G4_Water	Cell central				
Source	Nucl	Cyt(A)	Cyt(B)	CellM	Tot.
Nucl	14.89	20.56	25.85	10.37	71.69
Cyt(A)	2.91	24.95	38.27	9.01	75.15
Cyt(B)	0.48	5.49	51.94	12.25	70.18
CellM	0.15	1.59	19.32	32.74	53.81

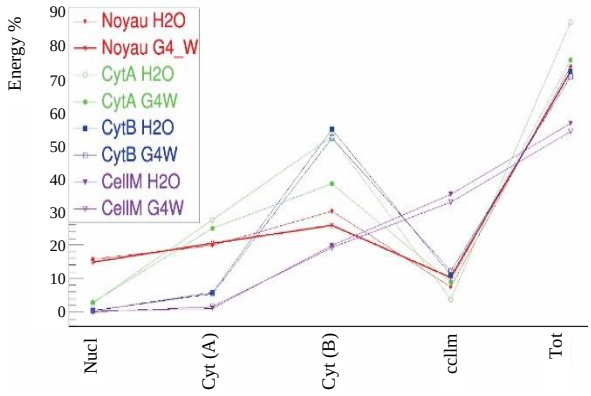

Fig. 28. Comparison of deposited energy percentages: H_2O vs G4_Water.

Energy deposition patterns using G4QGSP_BIC_HP physics List

Following our previous study, we have reproduced the simulations with a significant methodological change: the substitution of the Geant4-DNA physics list with the G4QGSP_BIC_HP (High Precision) list. This substitution allows us to assess the impact of the physics list on the simulation results. All other parameters, including the cellular geometry, water models (H_2O and G4_WATER), and the types of particles studied, remained identical to those in our initial study.

The results of these updated simulations are presented in Figs. 29-38, which illustrate the energy deposition profiles across different cellular compartments for various particle types.

Study system with Alpha particles

To complement these visual representations, the corresponding quantitative data are compiled in Table 3, The comparison between these two models enables the evaluation of how the choice of water model affects the energy deposition patterns.

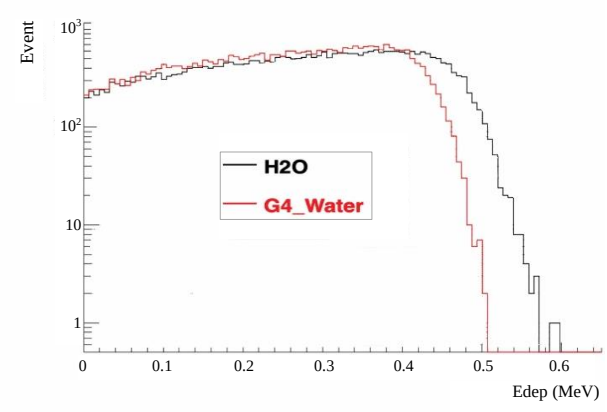

Fig. 29. Energy distribution in Nucleus: Nucleus source.

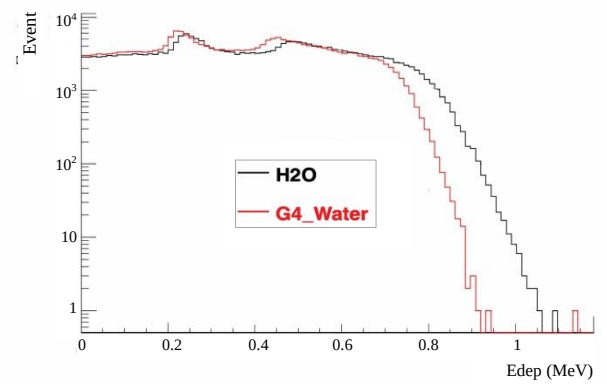

Fig. 30. Energy distribution in Cyto. A: Cyto. A source.

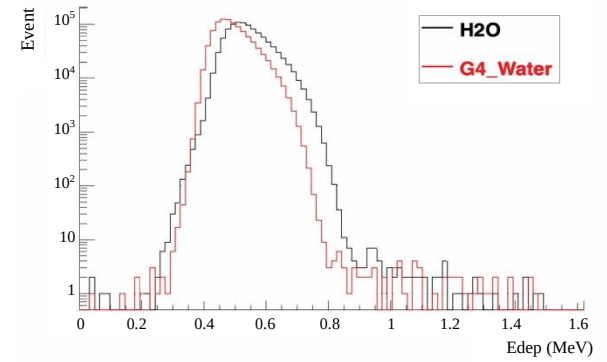

Fig. 31. Energy distribution in Cyto. B: Cyto. B source.

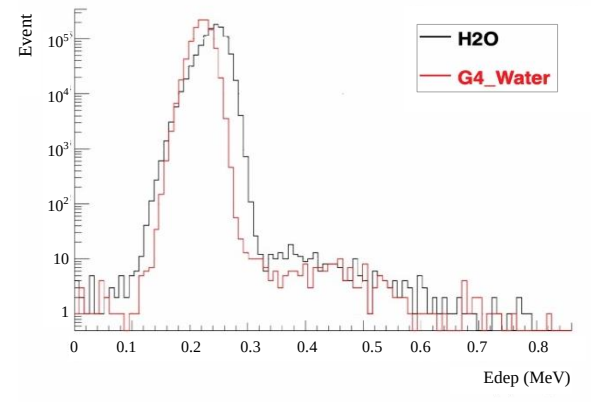

Fig. 32. Energy distribution in CellM: CellM source.

As shown in Tables 4 (a) and (b), significant variations in energy deposition are observed depending on the source location and target compartment. This comparative approach allows for a detailed analysis of the differences in energy deposition profiles and facilitates an assessment of the sensitivity of the results to both the selected physics list and the water model (Fig. 33).

Overall, the results obtained using H_2O and G4_WATER are generally consistent. The G4_WATER model consistently shows slightly lower percentages of deposited energy compared to the H_2O model.

Table 4a. Percentage of deposited energy using H_2O.

H_2O	Cell central				
Source	Nucl	Cyt(A)	Cyt(B)	CellM	Tot.
Nucl	10.46	16.96	33.44	15.98	76.85
Cyt(A)	3.44	18.37	38.86	16.03	74.12
Cyt(B)	0.94	6.29	37.43	18.20	62.88
CellM	0.61	4.12	27.37	21.45	53.56

Table 4b. Percentage of deposited energy using G4_Water.

G4_Water	Cell central				
Source	Nucl	Cyt(A)	Cyt(B)	CellM	Tot.
Nucl	9.73	15.67	30.32	14.75	70.48
Cyt(A)	3.17	16.99	33.10	14.95	68.23
Cyt(B)	0.87	5.79	34.79	17.23	58.69
CellM	0.56	3.79	25.58	20.29	50.23

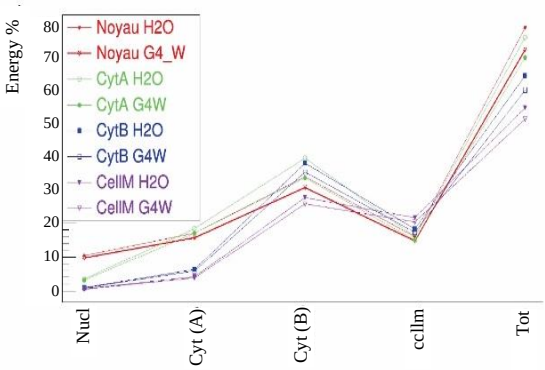

Fig . 33. Percentage of deposited energy: H_2O vs G4_Water.

Study system with lithium-ion

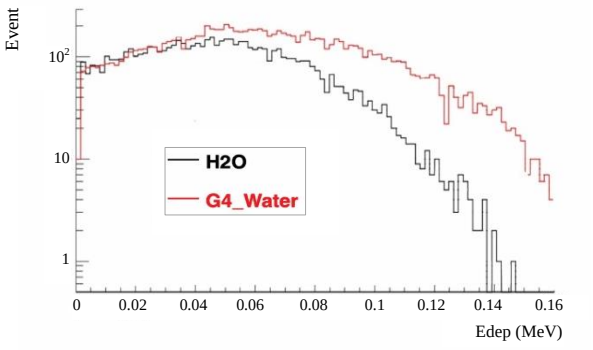

Fig. 34. Distribution of deposited energy in Nucleus: Nucleus source.

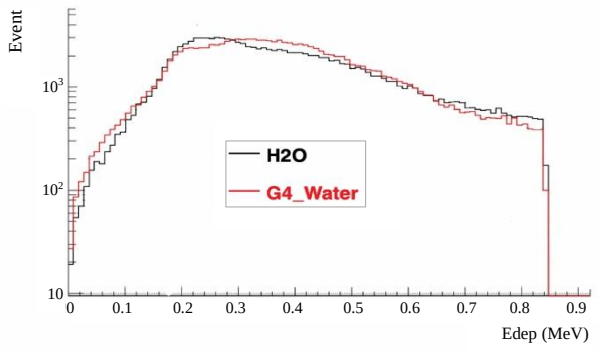

Fig. 35. Distribution of deposited energy in Cyto. A: Cyto. A source.

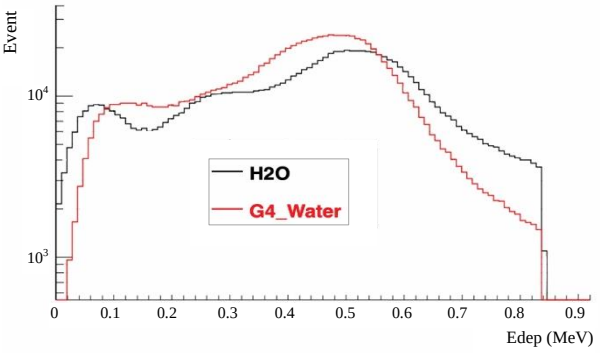

Fig. 36. Distribution of deposited energy in Cyto. B: Cyto. B source.

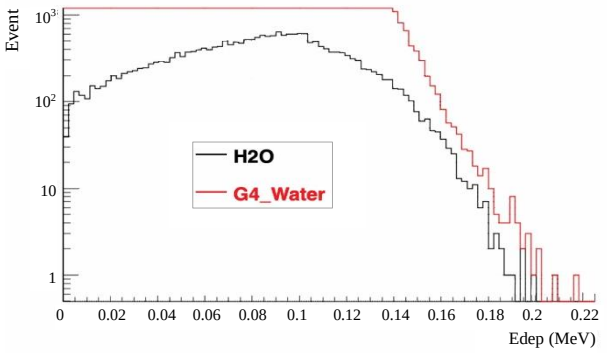

Fig. 37. Distribution of deposited energy in CellM: CellM source.

To quantify these results, we have compiled the percentage of energy deposited in each cellular compartment for different source positions in Table 5. This table is divided into two parts: Table 5 (a) presents the results using the H_2O model, while Table 5 (b) shows the results using the G4_WATER model. This side-by-side comparison allows us to assess the impact of water model choice on energy deposition patterns.

Furthermore, to visually represent the data from Tables 5 (a) and (b), we have created Fig. 38, which illustrates the percentage of energy deposited in each compartment for both water models. This plot provides a clear visual comparison of how the choice of water model affects energy deposition across different cellular compartments.

Table 5a. Percentage of deposited energy using H_2O.

H_2O	Cell central				
Source	Nucl	Cyt(A)	Cyt(B)	CellM	Tot.
Nucl	29.39	35.83	34.89	0.21	99.98
Cyt(A)	5.11	44.72	46.47	2.82	99.14
Cyt(B)	0.59	5.68	65.27	17.95	89.50
CellM	0.03	0.38	18.39	47.00	65.82

Table 5b. Percentage of deposited energy using G4_Water.

G4_Water	Cell central				
Source	Nucl	Cyt(A)	Cyt(B)	CellM	Tot.
Nucl	26.33	33.63	35.89	3.65	99.52
Cyt(A)	4.79	40.47	46.81	5.62	97.70
Cyt(B)	0.62	5.88	61.79	18.27	86.58
CellM	0.07	0.74	18.55	43.86	63.24

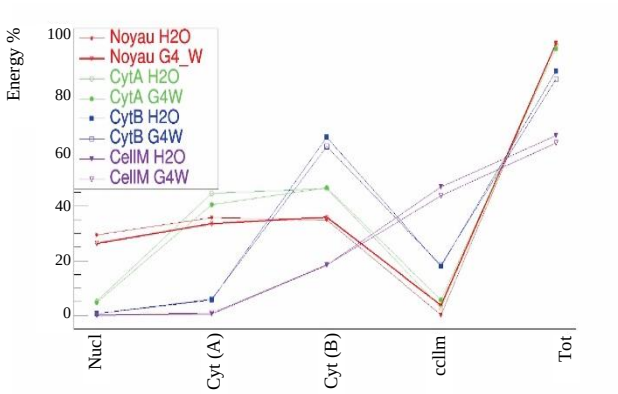

Fig. 38. Percentage of deposited energy: H_2O vs G4_Water**.**

In our simulations of the mono-cellular system using the G4QGSP_BIC_HP physics list, we observed distinct energy deposition patterns for alpha particles and lithium ions. These differences highlight the unique behaviors of these particles in cellular structures and their potential impacts on BNCT effectiveness.

DISCUSSION

The subtle differences identified between physics lists and water models in our Geant4 simulations, while seemingly minimal at first glance, are of crucial importance for precise Boron Neutron Capture Therapy (BNCT) treatment planning. Although these variations are on the order of a few percent, they can have significant repercussions on treatment efficacy and safety.

For example, in the context of brain tumor treatment, where millimeter precision is crucial, our simulations showed that the G4QGSP_BIC_HP physics list predicts slightly higher energy deposition in the cell nucleus compared to the Geant4-DNA physics list (a 3.2 % difference for alpha particles and 4.7 % difference for lithium-7 ions). This seemingly

minor divergence could critically influence the delineation of treatment areas. Even a small overestimation of 2-3 % in energy deposition could lead to an underestimation of the necessary dose at tumor edges, potentially compromising tumor control in these critical regions.

Moreover, these differences affect our understanding of particle range. The G4_WATER model produced slightly more diffuse energy deposition profiles than the H_2O model, with an average difference of 2.8 % in Bragg peak width. This variation could alter our estimation of particle travel distance within tissue. In the context where a brain tumor is near critical organs at risk, such as the brain stem, overestimating this diffusion could lead us to impose excessive dose restrictions, potentially reducing treatment effectiveness.

These variations also affect our calculation of the optimal boron concentration within the tumor. If our model underestimates energy deposition, we might be led to use a higher boron concentration than necessary. This could not only increase the risk of boron-related side effects but also alter the dose distribution between the tumor and surrounding healthy tissues. Conversely, overestimating energy deposition could lead to insufficient boron uptake, compromising the therapeutic efficacy of BNCT treatment [22].

It's crucial to note that these differences are not uniform across the simulated cellular geometry. For example, we observed that discrepancies between models were more pronounced in regions of high electron density, such as the cell nucleus, compared to the cytoplasm. This heterogeneity of differences underscores the importance of accurate subcellular-scale modeling for optimal BNCT treatment planning.

A thorough understanding of these model differences is, therefore, essential for several reasons: *Treatment plan optimization*, it allows us to finely adjust treatment parameters, such as neutron fluence and boron concentration, taking into account uncertainties related to the choice of physical model; *Risk assessment*, by better understanding variation in energy deposition, we can more accurately estimate risks surrounding healthy tissues, enabling a more balanced approach between therapeutic efficacy and minimizing the potential harm to organs at risk; *Treatment personalization*, by knowing the limitations and strengths of each model, we can adapt our approach based on the specific characteristics of each tumor and its location; *Model improvement*, this comparative study paves the way for future improvements in simulation models by identifying areas where greater precision is needed.

In conclusion, while these differences may seem subtle, they have profound implications for BNCT. They underscore the need for a rigorous and critical approach in interpreting simulation results for clinical BNCT treatment planning. This in-depth understanding allows us to develop more precise and personalized treatment plans for each patient, thus optimizing the effectiveness of cancer treatment while minimizing risks to healthy tissues.

CONCLUSION

This study has provided valuable insights into the microdosimetry of BNCT at the cellular level using high-fidelity Monte Carlo simulations. By comparing physics lists and water models in Geant4, we demonstrated consistent energy deposition predictions for alpha particles and lithium ions, validating the reliability of the applied models.

Notably, the water model influenced energy deposition only slightly, highlighting the importance of material definitions for reproducible BNCT simulations. Alpha particles showed localized energy deposition, particularly in the nucleus, while lithium ions exhibited a more diffuse pattern, especially within the cytoplasm. These findings emphasize the need for accurate lithium-ion modeling in BNCT dosimetry.

Our analysis across cellular compartments confirmed that the nucleus receives the highest energy dose, reinforcing the potential for DNA damage during BNCT. Furthermore, the results suggest that enhancing boron delivery to the nucleus could improve treatment effectiveness.

While this mono-cellular model offers important conclusions, future work should extend to multicellular simulations, heterogeneous boron distributions, and validation with experimental data to strengthen clinical relevance.

Overall, this study contributes to advancing BNCT treatment planning by clarifying the roles of alpha particles and lithium ions in cellular energy deposition and by guiding future simulation and experimental research.

FUTURE PERSPECTIVES

While our study focused on a monocellular model, extending this work to a multicellular model represents a crucial direction for future BNCT research. Such an extension would allow for a more

precise evaluation of the influence of alpha particles and lithium ions on neighboring cells, which is essential for understanding bystander effects and potential damage to adjacent healthy tissues. Specific areas for future investigation include: Development of a 3D geometric model incorporating multiple cells with varying boron concentrations to simulate tumor heterogeneity. Study of radiation damage propagation to non-targeted neighboring cells.

Analysis of the impact of different cellular configurations on overall BNCT treatment efficacy. Implementing such a multicellular model will present significant computational challenges, potentially requiring the use of optimization techniques and high-performance computing. However, the results could greatly aid in optimizing BNCT treatment planning by allowing for better prediction of damage to healthy tissues and more precise dosimetry.

This extension will necessitate close collaboration between medical physicists. Furthermore, a multicellular model could facilitate the study of integrating BNCT with other treatment modalities, such as chemotherapy or immunotherapy. In conclusion, while our current work provides valuable insights into BNCT microdosimetry at the cellular level, the development of multicellular models represents an exciting and necessary next step in advancing our understanding and optimization of this promising cancer treatment modality.

ACKNOWLEDGMENT

The authors would like to express their gratitude to the Laboratory of High Energy Physics and Condensed Matter, Faculty of Science Ain Chock, Hassan II University of Casablanca, Morocco, for providing the computational resources and facilities essential for this work. Special thanks are extended to the team members for their valuable discussions and technical support throughout the project.

AUTHOR CONTRIBUTION

K. Charef was the primary contributor to this work. Y. Khoulaki served as the overall supervisor of the study. The remaining authors contributed equally to the research and to the preparation of the manuscript.

REFERENCES

1. P. Maass, W. Dieterich, F. Scheffler, *Nearly Constant Loss Spectra in Glasses: Dipolar Interaction Effects*, in: AIP Conf. Proc. **832** (2006) 492.
2. M. Takagaki, W. Powell, A. Sood *et al*., Radiat. Res. **156** (2001) 118.
3. W. Sauerwein, A. Wittig, R. Moss *et al*., Springer-Verlag Berlin Heidelberg (2012) **1**.
4. J. Coderre and G. Morris, Radiat. Res. **151** (1999) 1.
5. A. Monti Hughes and N. Hu, Cancers **15** (2023) 4091.
6. K. Nedunchezhian, N. Aswath, M. Thiruppathy *et al.*, J. Clin. Diagn. Res. **10** (2016) ZE01.
7. D. Skwierawka, J. López-Valverde, M. Balcerzyk *et al*., Cancers **14** (2022) 2865.
8. A. Karaoglu, P. Arce, D. Obradors *et al*., Appl. Radiat. Isot. **132** (2018) 206.
9. A. Bahari, S. Mohammadi, N. Shakib *et al*., Atom Indones. **50** (2024) 27.
10. M. Ali, A. Abdel Monem, S.K. Elshamndy *et al.*, Atom Indones. **48** (2022) 237.
11. S. Santosa, K. Khotimah, and H. Yasmine, Atom Indones. **1** (2023) 97.
12. T. Mukawa, T. Matsumoto, K. Niita, Prog. Nucl. Sci. Technol. **2** (2011) 242.
13. I. Hrivnácová, and G. Barrand, EPJ Web Conf. **295** (2024) 03006.
14. T. Bakolia, D. Abdessamad, R. Sebihi *et al.*, Atom Indones. **1** (2024) 37.
15. S. Agostinelli, J. Allison,K. Amako *et al.*, Nucl. Instrum. Methods Phys. Res. A **506** (2003) 250.
16. A. Leyva and E. Munévar, Biophys. Rev. **15** (2023) 1.
17. S. Incerti, M. Douglass, S. Penfold *et al.*, Phys. Med. **32** (2016) 1187.
18. R. Tesse, F. Stichelbaut, N. Pauly *et al.*, Nucl. Instrum. Methods Phys. Res. B **416** (2018) 68.
19. W.-G. Shin, J. Ramos-Mendez, N.H. Tran *et al.*, Phys. Med. **88** (2021) 86.
20. Y. Lu, Z. Xu, L. Zhang *et al*., Nucl. Instrum. Methods Phys. Res. B **506** (2021) 8.
21. J. Hopewell, G. Morris, A. Schwint *et al*., Appl. Radiat. Isot. **69** (2011) 1756.
22. S. Kaur, K. Singh, Ann. Nucl. Energy **63** (2014) 350.